Biochimica et Biophysica Acta 1848 (2015) 2013–2021

Contents lists available at ScienceDirect

Biochimica et Biophysica Acta

journal homepage: www.elsevier.com/locate/bbamem

Structural features and dynamic investigations of the membrane-bound cytochrome P450 17A1

Ying-Lu Cui [a], Qiao Xue [a,b], Qing-Chuan Zheng [a,c,*], Ji-Long Zhang [a], Chui-Peng Kong [a], Jing-Rong Fan [a], Hong-Xing Zhang [a,**]

[a] International Joint Research Laboratory of Nano-micro Architecture Chemistry, State Key Laboratory of Theoretical and Computational Chemistry, Institute of Theoretical Chemistry, Jilin University, Changchun 130023, PR China
[b] State Key Laboratory of Environmental Chemistry and Ecotoxicology, Research Center for Eco-Environmental Sciences, Chinese Academy of Sciences, Beijing 10085, PR China
[c] Key Laboratory for Molecular Enzymology and Engineering of the Ministry of Education, Jilin University, Changchun 130023, PR China

ARTICLE INFO

Article history:
Received 25 December 2014
Received in revised form 4 May 2015
Accepted 19 May 2015
Available online 27 May 2015

Keywords:
Molecular dynamic
Cytochrome P450
Membrane-bound
Access tunnel

ABSTRACT

Cytochrome P450 (CYP) 17A1 is a dual-function monooxygenase with a critical role in the synthesis of many human steroid hormones. The enzyme is an important target for treatment of breast and prostate cancers that proliferate in response to estrogens and androgens. Despite the crystallographic structures available for CYP17A1, no membrane-bound structural features of this enzyme at atomic level are available. Accumulating evidence has indicated that the interactions between bounded CYPs and membrane could contribute to the recruitment of lipophilic substrates. To this end, we have investigated the effects on structural characteristics in the presence of the membrane for CYP17A1. The MD simulation results demonstrate a spontaneous insertion process of the enzyme to the lipid. Two predominant modes of CYP17A1 in the membrane are captured, characterized by the depths of insertion and orientations of the enzyme to the membrane surface. The measured heme tilt angles show good consistence with experimental data, thereby verifying the validity of the structural models. Moreover, conformational changes induced by the membrane might have impact on the accessibility of the active site to lipophilic substrates. The dynamics of internal aromatic gate formed by Trp220 and Phe224 are suggested to regulate tunnel opening motions. The knowledge of the membrane binding characteristics could guide future experimental and computational works on membrane-bound CYPs so that various investigations of CYPs in their natural, lipid environment rather than in artificially solubilized forms may be achieved.

1. Introduction

The CYPs are ubiquitous heme-containing mixed function oxygenases that catalyze the hydroxylation of non-activated hydrocarbon reactions, dealkylation, epoxidation, and dehydrogenation reactions involved in the oxidative metabolism [1–5]. They play an important role in the metabolism of endogenous and exogenous substrates like drugs and environmental chemicals [6,7]. The active site of CYPs is usually isolated from the surrounding solvent, and the heme cofactor is buried in the core of the enzymes [8]. Thus, the question of how reactants enter or exit the active site of the enzyme has become particularly important for membrane-associated CYPs.

CYPs are anchored in the membrane by an N-terminal TM α helix [9–14]. The heme tilt angle with respect to the membrane (the dihedral angle between the heme plane and the membrane plane) has been estimated experimentally to be between 38° and 78° for different CYP isoforms [15]. Recently, several groups have focused on the structural dynamics of the membrane-bound CYPs [10,16–23]. They used highly mobile membrane mimetic model/coarse grained simulations to observe the binding and insertion of CYPs, or initially immersed CYPs into the membrane to investigate the structural characteristics of the membrane-bound CYP isoforms. Accumulating evidence has discovered that the orientations may differ between individual CYPs, and some isoforms may even adopt different orientations in the membrane [10,11,15–24]. However, if different CYPs actually adopt different orientations in the membrane, the provided insightful information about the dynamics of the membrane-bound CYPs might be limited for other investigated isoforms, such as CYP17A1, an important target for the treatment of breast and prostate cancers.

CYP17A1 (also known as cytochrome P450c17) is a membrane-bound dual-function monooxygenase with a vital role in both adrenal and gonadal steroidogenesis in mammals [25,26]. As a key enzyme in

Abbreviations: CYP, cytochrome P450; MD, molecular dynamics; TM, transmembrane; POPC, 1-palmitoyl-2-oleoylphosphatidylcholine; PME, particle mesh Ewald; PO4, phosphorus; RMSD, root-mean-square deviations.

* Correspondence to: Q.C. Zheng, International Joint Research Laboratory of Nano-micro Architecture Chemistry, State Key Laboratory of Theoretical and Computational Chemistry, Institute of Theoretical Chemistry, Jilin University, Changchun 130023, PR China.
** Corresponding author.
E-mail address: zhengqc@jlu.edu.cn (Q.-C. Zheng).

http://dx.doi.org/10.1016/j.bbamem.2015.05.017
0005-2736/

the steroidogenic pathway, the 17α-hydroxylase/17, 20-lyase activities of CYP17A1 are required for the biosynthesis of androgenic steroids and estrogens in the adrenal zona reticularis and in gonads [27–29]. Given the fact that large number of lipophilic substrates metabolized by CYP17A1 primarily partition in the membrane, a daunting challenge is to provide the high-resolution structural determination of the membrane-associated state of CYP17A1. To this end, we have performed the full-atomistic MD simulations with lipid bilayer to study the binding and interaction of CYP17A1 to the membrane. The aims of this work are to answer the following questions: (i) what are the insertion depths and orientations of CYP17A1 on the membrane?, (ii) what are the key residues that may control the specific orientations of the globular domain of CYP17A1 to the membrane?, and (iii) what is the influence of the lipophilic environment of the membrane on the accessibility of the possible access tunnels? With multiple independent simulations, spontaneous insertion of the globular domain to the membrane has been captured, resulting in convergent models for the membrane-bound form of CYP17A1. The insertion orientations on the membrane show well agreement with the available experimental data [15]. Meanwhile, by using the full-atomistic MD simulations, a dynamic interacting procedure of the globular domain of CYP17A1 with the membrane was captured, which was not taken into account in previous simulations with simplified model of the lipid bilayer. These detailed membrane-induced hydrogen-bonding and hydrophobic interactions are inferred to anchor the protein within the membrane environment and to be closely relevant to control the pose of CYP17A1 on the membrane. Furthermore, the results suggest that the dynamics of aromatic residues may regulate the tunnel opening motions. The opening of tunnel 2fg was facilitated by the opening of the internal aromatic gate formed by Trp220 and Phe224. Together, the structural models resulting from the simulations allow for a detailed description of the structure–function relationships of CYP17A1 membrane-bound form, and could contribute to further understanding about the CYP17A1 associated polycystic ovary disease.

2. Computational methods

2.1. Preparation of the structure

Initial structure for CYP17A1 in complex with abiraterone was taken from Protein Data Bank (PDB ID: 3RUK). Structures for the N-terminal TM helix (Δ1–19 residues) and part of the Pro-rich loop (Δ20–30 residues), which are missing in the crystal structure, were modeled using Discovery Studio 3.0 [30]. Crystallographic water molecules were maintained. Abiraterone was removed from the prepared structure to obtain the substrate-free form of CYP17A1 for the subsequent docking study. The initial model of progesterone was obtained from DrugBank (http://www.drugbank.ca/; accession number: DB00396). CDOCKER protocol of Discovery Studio 3.0 [30] was used to create the docked CYP17A1–progesterone complex structure. Default settings for protein-small molecule docking were used. It is widely known that the heme group in iron(IV)–oxo heme(+·), or CpdI was considered to be the main reactive species of the CYP catalytic cycle [31–33]. Thus, in the present study, the active species of CYP17A1 was determined as iron–oxo-porphine complex, and the heme iron was ligated by the side chain thiolate group of the conserved cysteine residue (Cys442). The force field parameters of CpdI were obtained from previous QM/MM simulations reported by Cheatham et al. [34]. The structural optimization of progesterone was conducted using B3LYP combined with 6–31+G* basis set using the Gaussian 09 software [35]. RESP fitting procedure was used for charge derivation based on the optimal conformation. Finally, the force field parameters of progesterone were derived using the antechamber module of AMBER 11 [36].

2.2. MD simulations

For membrane-bound simulated systems, an explicit POPC bilayer [37] was used as a template to mimic the membrane environment because it is one of the major components of endoplasmic reticulum membrane (>50% phosphatidylcholine [38,39]). The TM helix was initially immersed into the POPC bilayer. The globular domain of CYP17A1–progesterone complex was placed in five different initial orientations, between 6 and 9 Å above the surface of the membrane. The initial orientations were obtained by first aligning the three principal axes of the protein to the xyz axes, respectively, and then rotating the principal axis aligned to z in different planes. In the present study, we obtained five different initial heme tilt angles. For comparison, CYP17A1 was also simulated in an aqueous solution. The systems were solvated with TIP3P water molecules and neutralized by chloride ions (Cl^-). All the atoms in the systems were described with AMBER [36,40] ff99SB force field [41]. GROMACS v4.6.5 [42] was used to run the simulations. Long range electrostatics were calculated using the PME method [43,44] with a 12 Å cut-off. Van der Waal interactions were modeled using Lennard–Jones 6–12 potentials with a 14 Å cut-off. All the simulations were conducted at a constant temperature of 300 K using the Berendsen thermostat. All bonds involving hydrogen atoms were constrained by the use of the SHAKE algorithm [45,46]. The time step in all MD simulations was set to 2 fs. Prior to production runs, energy minimization of 3000 steps of the steepest descent was carried out on each system followed by 5000 steps of conjugate gradient minimization. Subsequently, the minimized systems were heated gradually from 0 K to 300 K, and then equilibrated for a 1 ns NPT process. A 100 ns production run was conducted on each system, two of which were continued to 150 ns for further study.

The cluster analysis was performed using the average linkage as the clustering algorithm and backbone atom RMSD as the distance metric. The chosen of the representative structures can be summarized as follows: under the average linkage algorithm, the distance from one cluster to another is defined as the average of all distances between individual points of the two clusters. At each iteration step, the two closest clusters are merged. This merging continues until the desired number of clusters is obtained (here is 5). The representative structures of the clusters with the highest occurrences were chosen to present the structural information. All of the figures were created with Chimera [47].

2.3. New analysis of access tunnels

The access tunnels from the surface to the active site are very important for understanding the function of an enzyme [48]. In the present study, the transport pathways of CYP17A1 had been characterized by CAVER 3.0 [49,50]. Caver is a widely used software tool for automatic analyzing large ensembles of protein conformations [51–53]. The progesterone above the heme group was chosen as the starting point for tunnel searching. To investigate the opening of tunnels during the spontaneous binding and insertion of CYP17A1 into the membrane, 200 snapshots of each MD simulation trajectory were extracted at an interval of 500 ps. If the minimum radius of the segments along a tunnel was greater than 1.2 Å at least on snapshot of the simulations, the tunnel was collected. This value was chosen to be slightly lower than the usual probe radius of water of 1.5 Å because the radii calculated with the program are smaller than the actual radii of the tunnels. Then the identified tunnels of the last 50 ns MD simulations were characterized by the average-link algorithm based on the pairwise distances of the tunnels. The probe radius and the clustering threshold were set to 1.2 and 3.5, respectively. Default settings for other parameters were used throughout the calculations. The maximum number of tunnel clusters was set to 999. Then the tunnels were visualized using Chimera [47].

3. Results and discussion

3.1. Preparation for identifying the CYP17A1–progesterone complex structure

DeVore and Scott [25] determined the crystallographic structure of CYP17A1 with an inhibitor abiraterone to elucidate the structural features of this enzyme in 2012 (Fig. S1). However, no experimental crystallographic structures of CYP17A1–substrate complex are available in the course of our study. Thus, progesterone, which is the native CYP17A1 substrate, has been docked into the CYP17A1 substrate-free form to investigate the access of lipophilic substrate to the active site through the membrane. The metabolism of progesterone via CYP17A1 is essential for the biosynthesis of glucocorticoids and sex steroid precursors [54]. CYP17A1 can mediate 17-hydroxylation of progesterone to generate 17-OH progesterone, which can further be converted to glucocorticoids. After 17-hydroxylation, CYP17A1 also mediates the cleavage of the C17–C20 bond of 17-OH progesterone to form androstenedione, which is an important precursor for the production of estrogens and androgens [55]. Initial structure for CYP17A1 in complex with abiraterone was taken from Protein Data Bank (PDB ID: 3RUK) [25]. After docking, the conformation with the highest score among the captured complex conformations was chosen. Recently, Scott et al. [56] have also determined CYP17A1 mutant A105L with several substrates, including progesterone. Similar orientation and binding mode of the docked model of CYP17A1–progesterone complex were acquired compared to the newly crystallized structure proposed by Scott et al. [56] in their recent research (Fig. S2). The A ring of progesterone packs flat against the I helix and extends between the F and G helices. The distances between the protons of C17 and C16 atoms and the catalytic oxygen atom of CpdI were measured as about 2.65 Å (standard deviation: 0.21 Å) and 3.10 Å (0.37 Å) correspondingly throughout the last 50 ns simulations. The measured distances are consistent with the experimentally observed major 17α-OH and minor 16α-OH progesterone metabolites [25].

3.2. Spontaneous binding of the globular domain to the membrane and the orientations of the membrane-bound CYP17A1

After acquiring the complex structure of CYP17A1 with the lipophilic substrate, the TM helix of the enzyme was initially immersed into the POPC bilayer, whereas the globular domain was placed above the lipid bilayer at different orientations for five parallel MD simulations (Mem1 to Mem5). In the present study, the explicit POPC bilayer was used as a template to mimic the membrane environment because it is one of the major components of endoplasmic reticulum membrane (>50% phosphatidylcholine [38,39]). In the 100 ns simulations, spontaneous binding and immersion process of the globular domain to the membrane were consistently observed in all five simulations (Figs. 1 and S3).

The binding of the globular domain of CYP17A1 to the membrane was observed during the first 20 ns of the simulations independent of the globular domain's initial orientation. After membrane attachment, the globular domain of the enzyme oriented itself to a favorable position and penetrated into the membrane during approximately 20 to 50 ns of the MD simulations. Then, the orientation and the penetration depth for each simulated system did not significantly change over the remainder of the 100 ns MD simulations. Moreover, the TM helix displayed a small precession movement around the membrane normal inside the lipid bilayer. Finally, two distinct possible orientations were obtained from the MD simulations. From our simulations, the orientation of CYP17A1 after the association with the membrane was characterized by measuring the heme tilt angle with respect to the membrane normal (z-axis).

The initial and obtained average tilt angles for each simulated system are listed in Table 1. Time evolutions of the heme tilt angles for all simulated membrane systems (Mem1 to Mem5) are presented in Fig. 2. As shown in Fig. 2, all tilt angles rapidly changed during the first 50 ns. For the remainder of the simulations, the values averaged ~40° for Mem1 and Mem3, whereas they extended to much larger values between 58° and 65° for Mem2, Mem4, and Mem5, with an overall average of ~60°. In order to characterize the convergences of the distinct tilt angels, two of the simulations (Mem1 and Mem5) were extended to 150 ns. The results demonstrated that no large-scale tilting fluctuations between 40° and 60° were observed during the extended 50 ns of the simulations, indicating that two stable configurations were obtained from the MD simulations. Remarkably, the obtained two possible tilt angles are consistent with the experimental values as 47° or 63°[15], thereby verifying the validity of the structural models. In addition, such non-unique tilt angles of CYP17A1 are also observed in other CYP isoforms, such as P450c21, which has tilt angles as 38° or 78° [15]. Although two possible tilt angles were obtained for CYP17A1, the convergences of the two predominant orientations still suggest the specific orientations of CYP17A1 binding to the membrane, rather than a non-specific adsorption to the membrane surface.

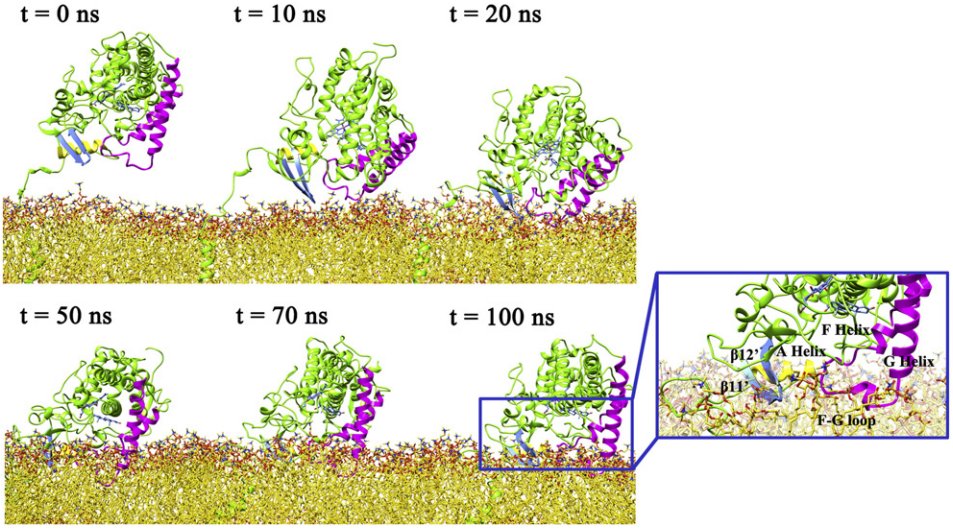

Fig. 1. Spontaneous binding and insertion of CYP17A1 into the membrane at different time points for the ~40° tilt angles membrane-bound systems. Close-up view of the membrane-bound form of CYP17A1, highlighting the regions having close contact with the membrane. The CpdI and progesterone are shown in blue stick representation. The F–G helices, A helix, and β11′–β12′ sheets are shown in ribbon representation in purple, yellow, and blue, respectively.

Table 1
Initial and average heme tilt angles calculated for all the simulated membrane-bound systems.

System	Initial tilt angle (degree)	Average tilt angel (degree)
Mem1	17.42	41.35 ± 3.28
Mem2	36.87	58.29 ± 3.29
Mem3	54.57	40.98 ± 3.54
Mem4	61.52	65.71 ± 3.70
Mem5	81.75	64.85 ± 3.55

3.3. Penetration of the globular domain of CYP17A1 into the membrane and the associated conformational changes

Fig. 3 summarizes the heights of the center of mass of the predominant anchorage regions in the globular domain of CYP17A1. Inspection of the trajectories revealed the penetration of the anchorage regions into the membrane before the formation of the enzyme–membrane complex. In general, the initial insertion began with the F–G loop, followed by the A helix and β11′–β12′ sheets in all simulated systems. More specifically, for the simulated systems with ~60° tilt angles, the penetration of the F and G helices occurred after the binding of the F–G loop, and these regions are proposed to be the primary attachment point for the globular domain of CYP17A1 to the membrane. Previous experimental study [15] has demonstrated that a considerable part of CYP17A1 is deeply embedded into the lipid bilayer. Larger tilt angle is inferred to penetrate more surface of the helix F–G region with its hydrophobic tip immersing deeper into the membrane. In the present study, the depths of insertion of the globular domain in the membrane were approximately 20–23 Å for simulations with ~60° tilt angles and 9–11 Å for ~40° tilt angle systems (Fig. S4A, B). As shown in Fig. S4, the globular domain of CYP17A1 was more inclined toward the membrane for the simulations with ~60° tilt angles. Consequently, the locations of β1 sheets (β11′, β12′, β13′, and β14′) relative to the membrane surface were slightly different, especially for β11′–β12′ sheets that were immersed below the lipid headgroups. In addition, β31′, β32′–β33′, and β41′–β42′ sheets were more immersed for the simulations with ~60° tilt angles as they made closer contact with the lipid bilayer. Although the regions including D, E, I, J, and K helices remained above the membrane, they located much closer to the membrane in ~60° tilt angle systems. However, the D–E loop and β3 sheets had no contact with the membrane for ~40° tilt angle systems. The F and G helices were observed to insert deeply into the membrane hydrophobic interior for the simulations with ~60° tilt angles, but to a lesser extent for ~40° tilt angle systems.

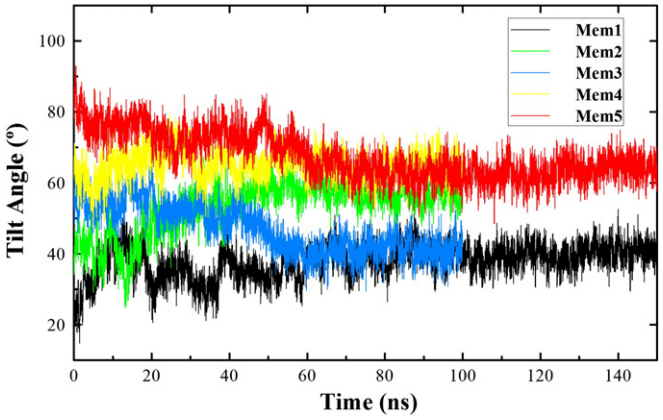

Fig. 2. Orientations of CYP17A1 upon binding to the membrane: time evolution of the heme tilt angle for the membrane-bound systems. The angle θ is defined as the angle between the membrane normal (z-axis) and the heme plane.

Fig. S5 shows the number of contacts between the protein residues and the lipids. Aliphatic residues (L, I and V) and aromatic residues (F, Y and W) preferred to penetrate deep into the membrane and contact with lipid tails, whereas charged (R, K, D and E) and polar residues (S, T, N and Q) mainly made contacts with the headgroup region. Hydrophobic and charged residues in contact with the lipids are demonstrated in Fig. S6. For the simulations with ~60° tilt angles, the globular domain of CYP17A1 exhibited larger contact surface with the lipids. The principal difference occurred on the helix F–G region, B–C loop, and the loop between β3 and β4 sheets, especially for the F–G region.

Significant local conformational changes at the membrane interface accompany the process of the protein insertion into the membrane. Fig. 4 demonstrates the membrane-induced conformational changes of the F–G helices hydrophobic tip, and the corresponding rearrangement of the key hydrophobic residues which interact with the lipid bilayer. For comparison, CYP17A1 was also simulated in an aqueous solution. The representative structures for the membrane-bound and solution form of CYP17A1 were superimposed with each other based on the Cα atoms of the globular domain of CYP17A1. As shown in Fig. 4, the conformational changes of the local structural motifs are compared to those in the solution simulation. With the immersion of the globular domain of CYP17A1, the F–G loop with its hydrophobic core composed of residues Leu214, Val215, Leu217, Val218, Trp220, Leu221, Ile223, and Phe224 inserted deeper into the membrane and extended away from the B–C loop. Other basic residues (Lys211, Lys227, Lys231, and Lys237) and polar residue Asn226 mainly interacted with the lipid headgroups. Concomitant movement of the G helix appeared to be associated with the extended conformational change of the F–G loop.

However, binding of CYP17A1 to the membrane does not induce any global conformational changes in the enzyme within the simulated time, as measured by the backbone RMSD with respect to their initial coordinates, which shows values <3.0 Å (Fig. S7). Another look at the plots in Fig. S8 points out the structural stability of the individual elements of secondary structure. As shown in Fig. S8, on average, the global secondary structures are well maintained over the 100 ns simulations. On the basis of the above structural analysis, the global protein structure and the overall topology for CYP17A1 are quite reserved upon binding to the membrane. Local conformational changes, which are mostly located at the membrane–protein interface, likely arise due to the interaction of CYP17A1 with the membrane, and may further impact on the opening and closing of different tunnels for efficient recruitment of the lipophilic substrates from the membrane to the enzyme's buried active site.

3.4. The details of insertion: membrane-induced interactions of the enzyme with lipid molecules

To further characterize the detailed interactions between CYP17A1 and membrane, we analyzed the hydrogen bonds, as well as the hydrophobic interactions formed between the residues and the lipid molecules in the membrane, in particular for the anchorage regions which penetrated into the lipid bilayer. In general, the predominant hydrogen-bonding interactions with the lipid molecules were either via basic residues (Lys and Arg) and polar residues (Ser, Thr, Gln, and Asn), or via the backbones of the hydrophobic residues (especially Leu and Phe) to a lesser extent. More specifically, Mem1 and Mem5 were taken as the representative systems of the two distinct orientations to demonstrate the detailed contacts of the protein with the membrane (Table S1). Time evolutions of the hydrogen bond occupancies are shown in Figs. 5 and S9. As shown in the hydrogen-bonding figures, residues Arg20, Arg21, and Lys26 were located in the Pro-rich loop and formed continuous hydrogen bonds with lipid bilayer during the simulation. These hydrogen bonds were relatively stable throughout the entire trajectory. Different from these fairly constant hydrogen bonds, some individual terms varied with their positions. With the

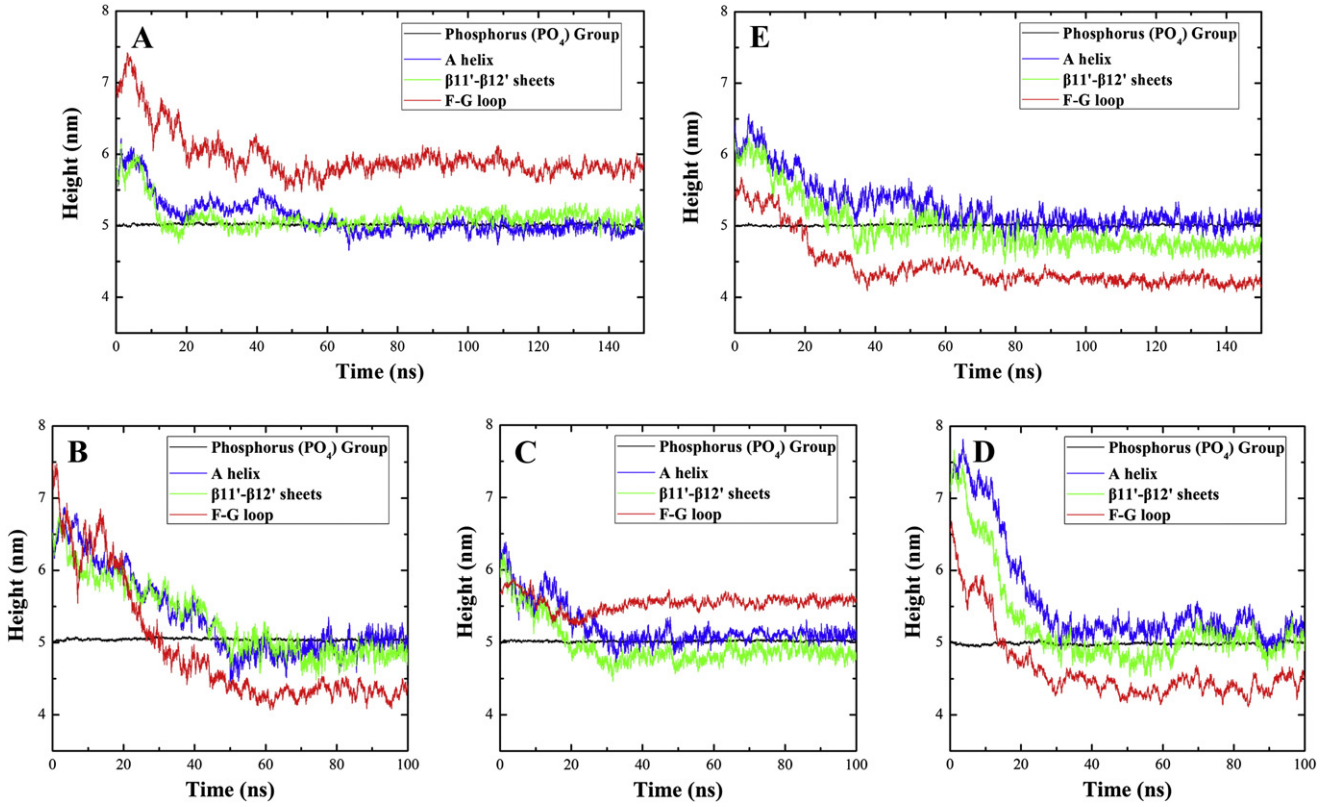

Fig. 3. Time series of the height of the center of mass of the A helix, β11′–β12′ sheets, and F–G helices in all five membrane simulations. The average positions of the PO4 group of the lipid headgroups are also shown.

immersion of CYP17A1 into the membrane, hydrogen bonds between the lipid headgroups and the residues located in specific regions were established, including the Pro-rich loop (Ser33, Leu34, Ser39, Leu40, Phe42, Leu43, and Arg45), B–C loop (Arg67 and Thr70), F–G loop (Lys211 and Lys231), and the loop between the β32′–β33′ sheets (Gln472 and Ser475). These hydrogen-bonding interactions remained bounded after 50 ns of the simulation.

Remarkably, the tilt angle was ~40° when Asn108, Arg109, Ser164, Lys237, and Lys490 were unable to form hydrogen bonds with the lipid headgroups, but it turned to be ~60° when these interactions were formed. In addition, lysine residue is known to bind either near the lipid tail or the headgroup interface, as it can create both favorable hydrogen bonds and hydrophobic interactions. In the present study, Asn226 and Lys227, which are located in the F–G loop, initially made contacts with the lipid headgroups by inserting the extended F–G loop into the lipid bilayer from solvent. However, when the tilt angle was ~60°, these two residues gradually lost the contact with the lipid headgroups as the globular domain inserted deeper into the membrane hydrophobic interior, and occasionally contacted the hydrophilic headgroups on the other side of the membrane. Then, new hydrogen bonds were intermittently formed.

In addition to the electrostatic interactions, the globular domain of CYP17A1 encountered the membrane mainly through the hydrophobic anchor of the F–G loop composed of Leu214, Val215, Leu217, Val218, Trp220, Leu221, Ile223, and Phe224 (Fig. 4). These nonpolar and aromatic residues formed predominantly hydrophobic interactions with the membrane lipid tails, contributing to the stability of CYP17A1 with the membrane. Other hydrophobic residues located in the anchorage regions (the Pro-rich loop, A helix, β1 and β3 sheets) could also participate in the hydrophobic contacts with the membrane to a lesser extent.

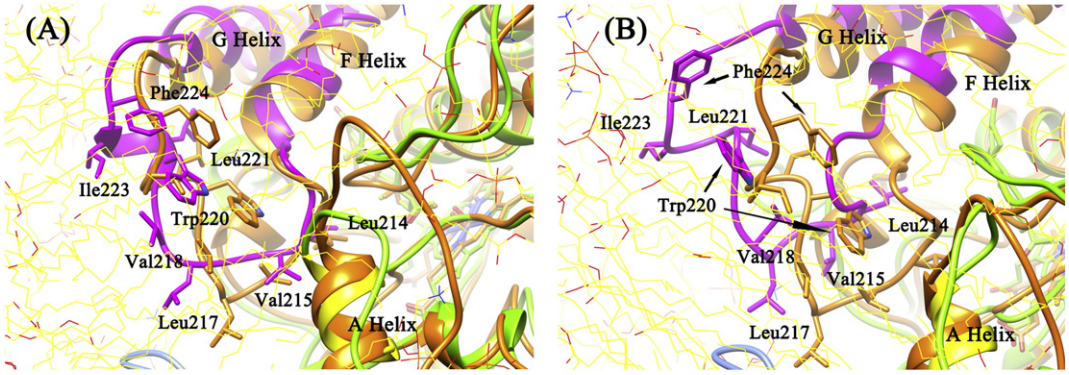

Fig. 4. Membrane-induced conformational changes of the hydrophobic tip of the helix F–G region for the membrane-bound systems with (A) ~40° tilt angles and (B) ~60° tilt angles. CYP17A1 in the membrane-bound form and in the solution form is shown in ribbon representation in green and dark yellow, representatively. F–G loop in the membrane-bound form is shown in purple ribbon representation. Hydrophobic residues are shown in stick representation. The lipid molecules in the membrane-bound form are shown in lines.

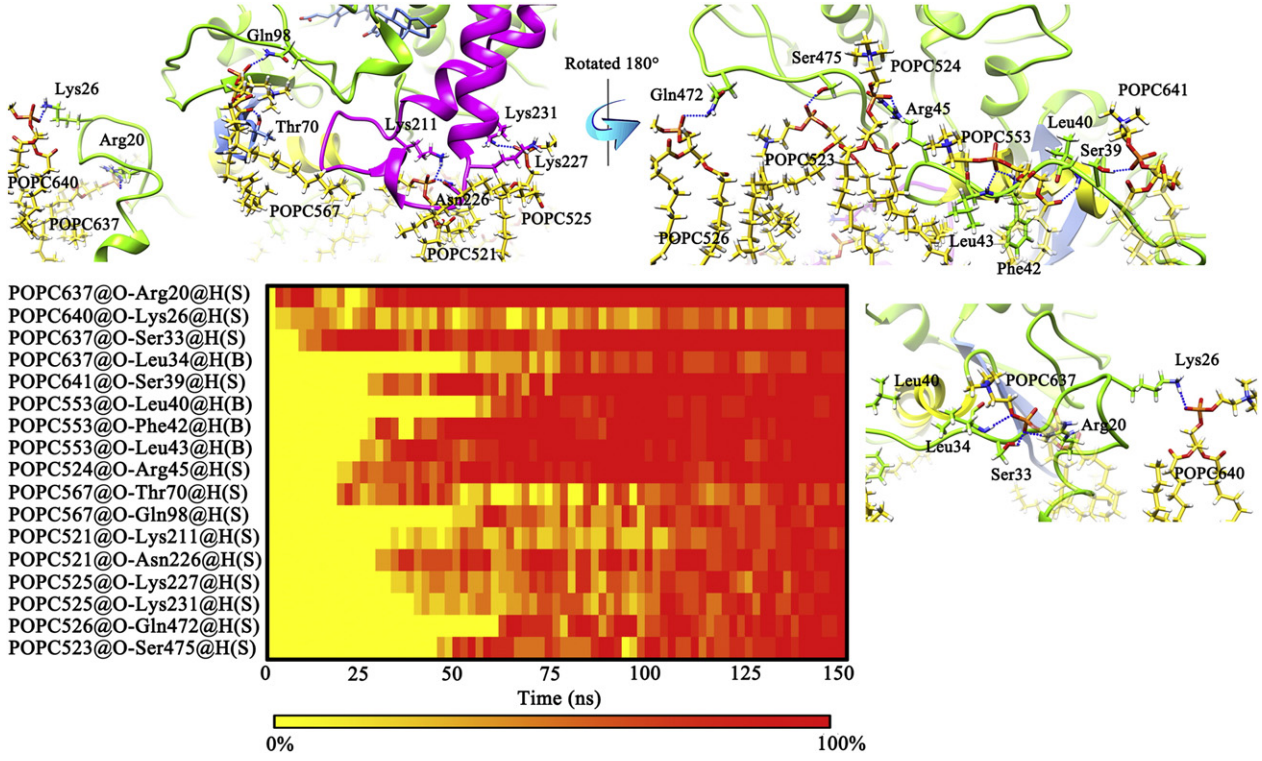

Fig. 5. Hydrogen-bonding interactions of the specific regions of CYP17A1 with the lipid molecules (top), and the time evolution of hydrogen bond occupancies of the lipids with the sidechains (S) and backbones (B) of the residues (bottom) for Mem1. CYP17A1 is shown in green ribbon representation. The F–G helices, A helix, and β11′–β12′ sheets are shown in ribbon representation in purple, yellow, and blue, respectively. Residues and lipid molecules are shown in stick representation. S and B represent the sidechain and backbone of the residue, respectively.

Overall, a great number of specific interactions identified to anchor the protein within the membrane environment have been suggested to be closely relevant to determine the well-defined orientations of CYP17A1 with respect to the membrane plane. The results indicate that CYP17A1 does not interact with the membrane merely through the simple nonspecific contacts, but rather through specific membrane–enzyme interactions that closely control the pose of the protein on the surface of the membrane. These hydrogen bonds together with the hydrophobic interactions are hypothesized to mediate the interactions of the globular domain of CYP17A1 with the membrane and may further have impact on the catalytic activity of CYP17A1 in the lipid bilayer.

3.5. Membrane-induced modulation of access tunnels

The active site of CYPs is usually isolated from the surrounding solvent, and buried in the core of the enzymes. The deeply buried active site points out the question of how molecular species enter the active site from protein surface through a series of access channels prior to reaction, a process that is particularly important for membrane-associated CYPs. Thus, the occurrences of tunnels in CYPs are highly concerned for its important role in protein engineering and drug design [57].

In our simulations, we have investigated the opening and closing motions of the substrate access tunnels induced by the interaction of CYP17A1 with the membrane, particularly for the tunnels facing the membrane. Multiple protein conformations were chosen to analyze the relevant features of individual transport tunnels in all membrane and solution simulations. Five top ranked tunnels identified throughout the MD simulations and their time evolution openings are all visualized in Fig. 6. Then the tunnels of the last 50 ns MD simulations were characterized by the average-link algorithm based on the pairwise distances of the tunnels. The characteristics of these tunnels are summarized in Table S2.

As shown in Fig. 6, the locations of the top ranked five tunnels are defined as 2f, S, 2b, 3, and 2fg. The nomenclature for these tunnels is identified systematically by Cojocaru et al. [57]. Tunnels 2f, 2b and 2fg are subclasses of tunnel 2. Tunnel 2f locates between the F–G loop, Pro-rich loop, and A helix, whereas tunnel 2b locates between the F–G loop and B–C loop. These pathways are relatively common in other cytochrome P450s [57–59]. However, tunnel 2fg, which has egress through the F–G loop, is rarely observed in other CYPs and serves as a newly dominant tunnel. Tunnel 3 locates between the F and G helices. It is identified as a potential secondary substrate/product egress route in MD simulations of P450cam [60]. The solvent tunnel (tunnel S), which runs between the E, F and I helices and β5 sheet, is proposed as a route for water to enter and leave the active site [57].

In the five membrane simulations, the main opening movement which is necessary for the substrate binding and product release is commonly associated with the F–G region. Tunnels 2f, 2fg, and 2b were observed to open to various degrees and penetrate into the lipid bilayer with the protein hydrophobic residues in the F–G loop interacting with the lipids. The slight movement of the G helix toward the lipids was suggested to mediate the wider opening of tunnel 2f during the last 50 ns of the membrane simulations. Remarkably, an alternative pathway through the tunnel 2fg was significantly more open in the membrane simulations. It is suggested that the interaction of CYP17A1 with the membrane would favor the opening of tunnel 2fg by extending the F–G loop into the hydrophobic interior. By comparing the residues in the membrane-bound form and in the solution form, the opening of tunnel 2fg is inferred to be promoted by the opening of the internal aromatic gate formed by Trp220 and Phe224 in the membrane-bound form, whereas the entrance of this tunnel in the solution form was partially locked by the steric hindrance of the side chains of these residues (Fig. 4). Moreover, tunnels 2f and 2fg were observed to open wider in the membrane-bound form systems with ~60° tilt angles than in the systems with ~40° tilt angles except for system Mem2. The more

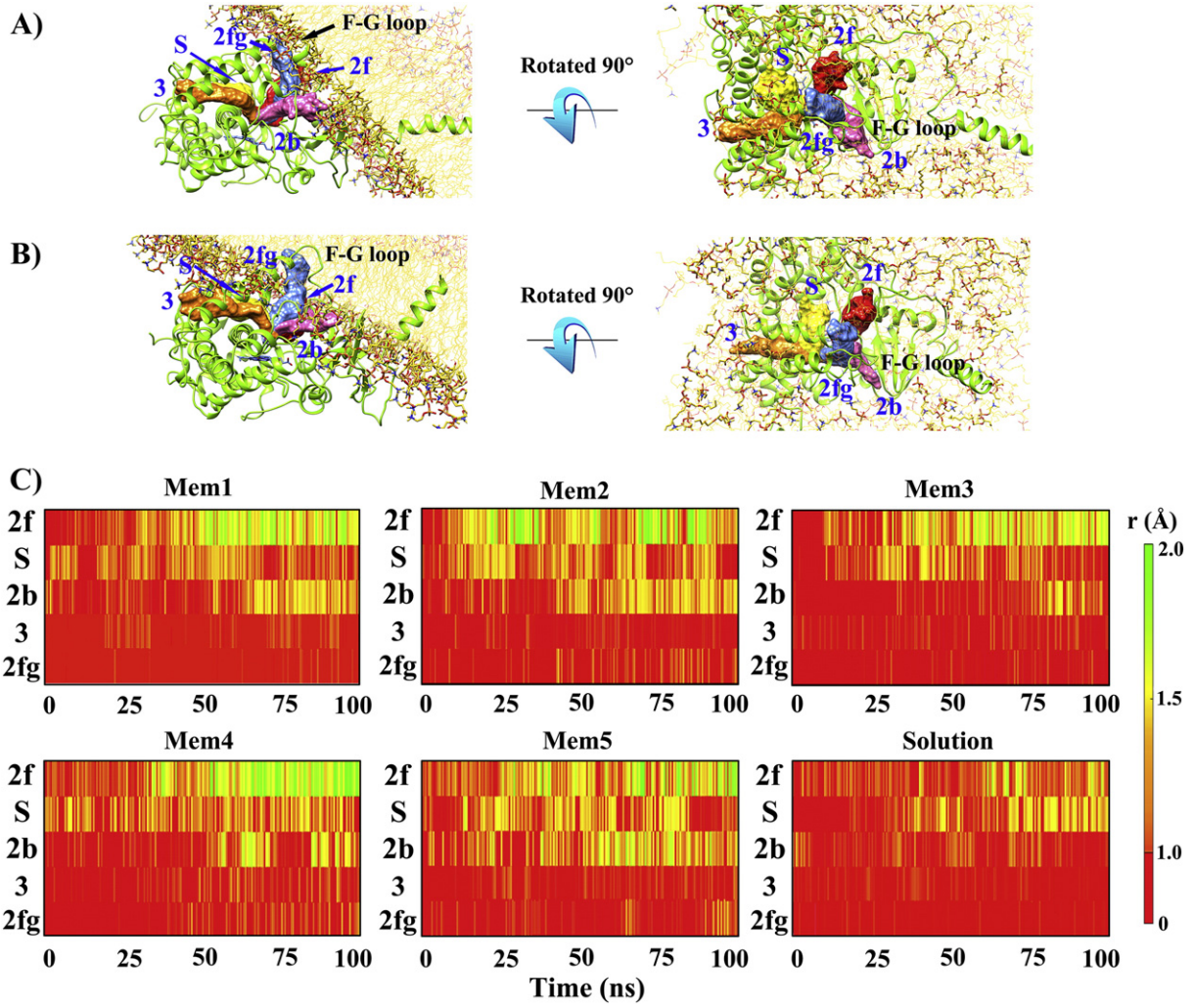

Fig. 6. Membrane-induced rearrangement of the access tunnels. Five top ranked collective pathways identified throughout the MD simulations are all depicted in one frame as pathway surfaces for the membrane-bound systems with (A) ~40° tilt angles and (B) ~60° tilt angles. Pathways following the ranking order are shown as red, yellow, pink, orange, and blue surfaces, respectively. (C) Time evolution between the opening and closing of different pathways during the membrane-bound and solution simulations. The color map ranges from very narrow (orange) to wide (green) bottlenecks.

opening of 2fg was also correlated with the opening of tunnel 2b, which was facilitated by the extended motion of the F–G loop away from the B–C loop.

Different from these tunnels which are facing the membrane, the opening and closing motions of tunnel 3 and tunnel S seemed to be independent of the conformations of the F–G loop, as well as the presence of the membrane. These two tunnels were intermittently opening throughout the membrane-bound and solution simulations. Thus, it is inferred that the rearrangement of the F–G region in the membrane-bound simulations is directly relevant to the opening and closing of the access tunnels facing the lipid layer, and may further influence the recruitment of lipophilic substrates from the membrane into the active site.

It should be noted that although these tunnels are significant for the recruitment of lipophilic substrates, the complete process and the ultimate open configuration of these tunnels have not been captured. The simulations are performed with the substrate in the active site of the enzyme. In this form, the complex structures are usually in closed conformation. The radii of the observed tunnels are still too small for some large substrates, indicating that further changes are needed to accommodate the substrates. The present study provides the main potential pathways in the closed form of the protein.

4. Conclusion

In conclusion, our present study indicates the value in modeling and simulating CYPs in their native, membrane-bound cellular environment. An important caveat for the investigation of CYPs is the fact that most studies appear to provide simulations in their solution form without taking into account the interaction of the enzyme with membrane, which could affect structural and dynamical characteristics of the enzyme. In the present study, we have constructed the structural models for the membrane-bound state of CYP17A1. The simulations resulted in convergent models of spontaneous binding and insertion of the globular domain of CYP17A1, characterized by the depths of insertion and orientations of the globular domain on the membrane surface. Remarkably, two predominant orientations captured in the five membrane-bound simulations provide a good consistence with the experiment data, which further verifies the validity of our structural models. The detailed hydrogen-bonding and hydrophobic interactions provide an important suggestion that the CYP17A1 may interact with the membrane through specific membrane–enzyme interactions that stabilize the binding mode of the protein with the membrane, rather than simply through the adsorption to the surface. Furthermore, the membrane binding of CYP17A1 has significant structural and dynamical

impacts on its globular domain at the membrane interface, that the primarily conformational changes of specific regions may play an important role in the opening and closing of different tunnels for efficient recruitment of lipophilic substrates from the membrane to the enzyme's buried active site. The dynamics of the aromatic residues are suggested to regulate tunnel opening motions. The opening of 2fg was facilitated by the opening of the internal aromatic gate formed by Trp220 and Phe224. Such structural characteristics are associated with the fact that the recruitment and binding of substrates are directly through the membrane into the active site of the enzyme. In summary, our present work provides detailed atomistic insights into the effects of the presence of the membrane on the structural and dynamical properties of CYP17A1. The knowledge of the membrane binding characteristics could guide future experimental and computational works on membrane-bound CYPs so that various investigations of CYPs in their native, membrane-bound cellular environment may be achieved.

Conflict of interest

The authors declare no competing financial interest.

Acknowledgement

This work is supported by the National Natural Science Foundation of China (grant no. 21273095).

Appendix A. Supplementary data

Supplementary data to this article can be found online at http://dx.doi.org/10.1016/j.bbamem.2015.05.017.

References

[1] P.R. Ortiz de Montellano, Hydrocarbon hydroxylation by cytochrome P450 enzymes, Chem. Rev. 110 (2009) 932–948.
[2] Y.L. Cui, Q.C. Zheng, J.L. Zhang, H.X. Zhang, Molecular basis of the recognition of arachidonic acid by cytochrome P450 2E1 along major access tunnel, Biopolymers 103 (2015) 53–66.
[3] Y.L. Cui, J.L. Zhang, Q.C. Zheng, R.J. Niu, Y. Xu, H.X. Zhang, C.C. Sun, Structural and dynamic basis of human cytochrome P450 7B1: a survey of substrate selectivity and major active site access channels, Chem. Eur. J. 19 (2013) 549–557.
[4] X.Y. Meng, Q.C. Zheng, H.X. Zhang, A comparative analysis of binding sites between mouse CYP2C38 and CYP2C39 based on homology modeling, molecular dynamics simulation and docking studies, BBA-Proteins Proteomics 1794 (2009) 1066–1072.
[5] M.K. Pandey, S. Vivekanandan, S. Ahuja, R. Huang, S.-C. Im, L. Waskell, A. Ramamoorthy, Cytochrome-P450–cytochrome-b 5 interaction in a membrane environment changes 15N chemical shift anisotropy tensors, J. Phys. Chem. B 117 (2013) 13851–13860.
[6] U.H. Dürr, L. Waskell, A. Ramamoorthy, The cytochromes P450 and b_5 and their reductases—promising targets for structural studies by advanced solid-state NMR spectroscopy, Biochim. Biophys. Acta Biomembr. 1768 (2007) 3235–3259.
[7] G. Lorbek, M. Lewinska, D. Rozman, Cytochrome P450s in the synthesis of cholesterol and bile acids—from mouse models to human diseases, FEBS J. 279 (2012) 1516–1533.
[8] R.C. Wade, P.J. Winn, I. Schlichting, A survey of active site access channels in cytochromes P450, J. Inorg. Biochem. 98 (2004) 1175–1182.
[9] T.L. Poulos, E.F. Johnson, Structures of cytochrome P450 enzymes, Cytochrome P450, Springer 2005, pp. 87–114.
[10] V. Cojocaru, K. Balali-Mood, M.S. Sansom, R.C. Wade, Structure and dynamics of the membrane-bound cytochrome P450 2C9, PLoS Comput. Biol. 7 (2011) e1002152.
[11] S.D. Black, Membrane topology of the mammalian P450 cytochromes, FASEB J. 6 (1992) 680–685.
[12] K. Yamamoto, M. Gildenberg, S. Ahuja, S.-C. Im, P. Pearcy, L. Waskell, A. Ramamoorthy, Probing the Transmembrane Structure and Topology of Microsomal Cytochrome-p450 by Solid-state NMR on Temperature-resistant Bicelles, Scientific Reports, 3, 2013.
[13] K. Yamamoto, U.H. Dürr, J. Xu, S.-C. Im, L. Waskell, A. Ramamoorthy, Dynamic Interaction Between Membrane-bound Full-length Cytochrome P450 and Cytochrome b5 Observed by Solid-state NMR Spectroscopy, Scientific Reports, 3, 2013.
[14] S. Ahuja, N. Jahr, S.-C. Im, S. Vivekanandan, N. Popovych, S.V. Le Clair, R. Huang, R. Soong, J. Xu, K. Yamamoto, A model of the membrane-bound cytochrome b5-cytochrome P450 complex from NMR and mutagenesis data, J. Biol. Chem. 288 (2013) 22080–22095.
[15] Y. Ohta, S. Kawato, H. Tagashira, S. Takemori, S. Kominami, Dynamic structures of adrenocortical cytochrome P-450 in proteoliposomes and microsomes: protein rotation study, Biochemistry 31 (1992) 12680–12687.
[16] K. Berka, T. Hendrychová, P. Anzenbacher, M. Otyepka, Membrane position of ibuprofen agrees with suggested access path entrance to cytochrome P450 2C9 active site, J. Phys. Chem. A 115 (2011) 11248–11255.
[17] I. Denisov, A. Shih, S. Sligar, Structural differences between soluble and membrane bound cytochrome P450s, J. Inorg. Biochem. 108 (2012) 150–158.
[18] J.L. Baylon, I.L. Lenov, S.G. Sligar, E. Tajkhorshid, Characterizing the membrane-bound state of cytochrome P450 3A4: structure depth of insertion and orientation, J. Am. Chem. Soc. 135 (2013) 8542–8551.
[19] K. Berka, M.t. Paloncýová, P. Anzenbacher, M. Otyepka, Behavior of human cytochromes P450 on lipid membranes, J. Phys. Chem. B 117 (2013) 11556–11564.
[20] J. Park, L. Czapla, R.E. Amaro, Molecular simulations of aromatase reveal new insights into the mechanism of ligand binding, J. Chem. Inf. Model. 53 (2013) 2047–2056.
[21] J. Sgrignani, A. Magistrato, Influence of the membrane lipophilic environment on the structure and on the substrate access/egress routes of the human aromatase enzyme. A computational study, J. Chem. Inf. Model. 52 (2012) 1595–1606.
[22] J. Sgrignani, M. Bon, G. Colombo, A. Magistrato, Computational approaches elucidate the allosteric mechanism of human aromatase inhibition: a novel possible route to small-molecule regulation of CYP450s activities? J. Chem. Inf. Model. 54 (2014) 2856–2868.
[23] R. Lonsdale, S.L. Rouse, M.S.P. Sansom, A.J. Mulholland, A multiscale approach to modelling drug metabolism by membrane-bound cytochrome P450 enzymes, PLoS Comput. Biol. 10 (2014) e1003714.
[24] K. Yamamoto, P. Pearcy, A. Ramamoorthy, Bicelles exhibiting magnetic alignment for a broader range of temperatures: a solid-state NMR study, Langmuir 30 (2014) 1622–1629.
[25] N.M. DeVore, E.E. Scott, Structures of cytochrome P450 17A1 with prostate cancer drugs abiraterone and TOK-001, Nature 482 (2012) 116–119.
[26] A.C. Swart, K.H. Storbeck, P. Swart, A single amino acid residue, Ala 105, confers 16α-hydroxylase activity to human cytochrome P450 17α-hydroxylase/17, 20 lyase, J. Steroid Biochem. Mol. Biol. 119 (2010) 112–120.
[27] A. Patocs, I. Liko, I. Varga, P. Gergics, A. Boros, L. Futo, I. Kun, R. Bertalan, S. Toth, T. Pazmany, M. Toth, N. Szucs, J. Horanyi, E. Glaz, K. Racz, Novel mutation of the CYP17 gene in two unrelated patients with combined 17 alpha-hydroxylase/17,20-lyase deficiency: demonstration of absent enzyme activity by expressing the mutant CYP17 gene and by three-dimensional modeling, J. Steroid Biochem. Mol. Biol. 97 (2005) 257–265.
[28] E.L.T. van den Akker, J.W. Koper, A.L.M. Boehmer, A.P.N. Themmen, M. Verhoef-Post, M.A. Timmerman, B.J. Otten, S.L.S. Drop, F.H. De Jong, Differential inhibition of 17α-hydroxylase and 17, 20-lyase activities by three novel missense CYP17 mutations identified in patients with P450c17 deficiency, J. Clin. Endocrinol. Metab. 87 (2002) 5714–5721.
[29] A. Di Cerbo, A. Biason-Lauber, M. Savino, M.R. Piemontese, A. Di Giorgio, M. Perona, A. Savoia, Combined 17α-hydroxylase/17, 20-lyase deficiency caused by Phe93Cys mutation in the CYP17 gene, J. Clin. Endocrinol. Metab. 87 (2002) 898–905.
[30] Discovery Studio, Version 3.0, Accelrys Software Inc., San Diego, CA, 2010.
[31] A. Seifert, S. Tatzel, R.D. Schmid, J. Pleiss, Multiple molecular dynamics simulations of human p450 monooxygenase CYP2C9: the molecular basis of substrate binding and regioselectivity toward warfarin, Proteins: Struct., Funct., Bioinf. 64 (2006) 147–155.
[32] K. Sen, J.C. Hackett, Molecular oxygen activation and proton transfer mechanisms in lanosterol 14α-demethylase catalysis, J. Phys. Chem. B 113 (2009) 8170–8182.
[33] K.P. Conner, C.M. Woods, W.M. Atkins, Interactions of cytochrome P450s with their ligands, Arch. Biochem. Biophys. 507 (2011) 56–65.
[34] K. Shahrokh, A. Orendt, G.S. Yost, T.E. Cheatham, Quantum mechanically derived AMBER-compatible heme parameters for various states of the cytochrome P450 catalytic cycle, J. Comput. Chem. 33 (2012) 119–133.
[35] M. Frisch, H. GWT, G. Schlegel, M. Scuseria, J. Robb, G.S. Cheeseman, V. Barone, B. Mennucci, G. Petersson, H. Nakatsuji, Gaussian 09 2009, Gaussian, Inc., Wallingford, CT, 2009.
[36] D. Case, T. Darden, T. Cheatham III, C. Simmerling, J. Wang, R. Duke, R. Luo, R. Walker, W. Zhang, K. Merz, AMBER 11, University of California, San Francisco, 142, 2010.
[37] A.-S. Schillinger, C. Grauffel, H.M. Khan, Ø. Halskau, N. Reuter, Two homologous neutrophil serine proteases bind to POPC vesicles with different affinities: when aromatic amino acids matter, Biochim. Biophys. Acta Biomembr. 1838 (2014) 3191–3202.
[38] M. Deleu, J.-M. Crowet, M.N. Nasir, L. Lins, Complementary biophysical tools to investigate lipid specificity in the interaction between bioactive molecules and the plasma membrane: a review, Biochim. Biophys. Acta Biomembr. 1838 (2014) 3171–3190.
[39] G. Van Meer, D.R. Voelker, G.W. Feigenson, Membrane lipids: where they are and how they behave, Nat. Rev. Mol. Cell Biol. 9 (2008) 112–124.
[40] Q. Xue, J.-L. Zhang, Q.-C. Zheng, Y.-L. Cui, L. Chen, W.-T. Chu, H.-X. Zhang, Exploring the molecular basis of dsRNA recognition by Mss116p using molecular dynamics simulations and free-energy calculations, Langmuir 29 (2013) 11135–11144.
[41] V. Hornak, R. Abel, A. Okur, B. Strockbine, A. Roitberg, C. Simmerling, Comparison of multiple AMBER force fields and development of improved protein backbone parameters, Proteins: Struct., Funct., Bioinf. 65 (2006) 712–725.
[42] B. Hess, C. Kutzner, D. Van Der Spoel, E. Lindahl, GROMACS 4: algorithms for highly efficient, load-balanced, and scalable molecular simulation, J. Chem. Theory Comput. 4 (2008) 435–447.
[43] Q. Xue, Q.C. Zheng, J.L. Zhang, Y.L. Cui, H.X. Zhang, Exploring the mechanism how Marburg virus VP35 recognizes and binds dsRNA by molecular dynamics simulations and free energy calculations, Biopolymers 101 (2014) 849–860.
[44] P.A. Kollman, I. Massova, C. Reyes, B. Kuhn, S. Huo, L. Chong, M. Lee, T. Lee, Y. Duan, W. Wang, Calculating structures and free energies of complex molecules: combining molecular mechanics and continuum models, Acc. Chem. Res. 33 (2000) 889–897.

[45] Q. Xue, Q.-C. Zheng, J.-L. Zhang, Y.-L. Cui, W.-T. Chu, H.-X. Zhang, Mutation and low pH effect on the stability as well as unfolding kinetics of transthyretin dimer, Biophys. Chem. 189 (2014) 8–15.
[46] J.-P. Ryckaert, G. Ciccotti, H.J. Berendsen, Numerical integration of the cartesian equations of motion of a system with constraints: molecular dynamics of *n*-alkanes, J. Comput. Phys. 23 (1977) 327–341.
[47] E.F. Pettersen, T.D. Goddard, C.C. Huang, G.S. Couch, D.M. Greenblatt, E.C. Meng, T.E. Ferrin, UCSF chimera—a visualization system for exploratory research and analysis, J. Comput. Chem. 25 (2004) 1605–1612.
[48] X. Yu, V. Cojocaru, R.C. Wade, Conformational diversity and ligand tunnels of mammalian cytochrome P450s, Biotechnol. Appl. Biochem. 60 (2013) 134–145.
[49] M. Petřek, M. Otyepka, P. Banáš, P. Košinová, J. Koča, J. Damborský, CAVER: a new tool to explore routes from protein clefts, pockets and cavities, BMC Bioinf. 7 (2006) 316.
[50] E. Chovancova, A. Pavelka, P. Benes, O. Strnad, J. Brezovsky, B. Kozlikova, A. Gora, V. Sustr, M. Klvana, P. Medek, CAVER 3.0: a tool for the analysis of transport pathways in dynamic protein structures, PLoS Comput. Biol. 8 (2012) e1002708.
[51] R. Blomberg, H. Kries, D.M. Pinkas, P.R. Mittl, M.G. Grütter, H.K. Privett, S.L. Mayo, D. Hilvert, Precision is essential for efficient catalysis in an evolved Kemp eliminase, Nature 503 (2013) 418–421.
[52] T. Ogawa, K. Noguchi, M. Saito, Y. Nagahata, H. Kato, A. Ohtaki, H. Nakayama, N. Dohmae, Y. Matsushita, M. Odaka, Carbonyl sulfide hydrolase from *Thiobacillus thioparus* strain THI115 is one of the β-carbonic anhydrase family enzymes, J. Am. Chem. Soc. 135 (2013) 3818–3825.
[53] Y.-L. Cui, Q.-C. Zheng, J.-L. Zhang, Q. Xue, Y. Wang, H.-X. Zhang, Molecular dynamic investigations of the mutational effects on structural characteristics and tunnel geometry in CYP17A1, J. Chem. Inf. Model. 53 (2013) 3308–3317.
[54] D.W. Nebert, D.W. Russell, Clinical importance of the cytochromes P450, Lancet 360 (2002) 1155–1162.
[55] N. Hinfray, D. Baudiffier, M.C. Leal, J.-M. Porcher, S. Aït-Aïssa, F. Le Gac, R.W. Schulz, F. Brion, Characterization of testicular expression of P450 17α-hydroxylase, 17, 20-lyase in zebrafish and its perturbation by the pharmaceutical fungicide clotrimazole, Gen. Comp. Endocrinol. 174 (2011) 309–317.
[56] E.M. Petrunak, N.M. DeVore, P.R. Porubsky, E.E. Scott, Structures of human steroidogenic cytochrome P450 17A1 with substrates, J. Biol. Chem. 289 (2014) 32952–32964.
[57] V. Cojocaru, P.J. Winn, R.C. Wade, The ins and outs of cytochrome P450s, Biochim. Biophys. Acta 1770 (2007) 390–401.
[58] K. Schleinkofer, P.J.W. Sudarko, S.K. Lüdemann, R.C. Wade, Do mammalian cytochrome P450s show multiple ligand access pathways and ligand channelling? EMBO Rep. 6 (2005) 584–589.
[59] D.C. Haines, D.R. Tomchick, M. Machius, J.A. Peterson, Pivotal role of water in the mechanism of P450BM-3, Biochemistry 40 (2001) 13456–13465.
[60] S.K. Lüdemann, V. Lounnas, R.C. Wade, How do substrates enter and products exit the buried active site of cytochrome P450cam? 1 Random expulsion molecular dynamics investigation of ligand access channels and mechanisms, J. Mol. Biol. 303 (2000) 797–811.